Simultaneous co-overexpression of *Saccharomyces cerevisiae* septins Cdc3 and Cdc10 drives pervasive, phospholipid- and tag-dependent plasma membrane localization

Aleyna Benson¹ and Michael McMurray¹,*

Affiliations

¹Department of Cell and Developmental Biology, University of Colorado Anschutz Medical Campus, Aurora, Colorado, United States of America

*Correspondence

Dr. Michael McMurray
Department of Cell and Developmental Biology
University of Colorado Anschutz Medical Campus
12801 E 17th Ave
RC1S Room 12117
Aurora, CO 80045, United States of America

Running title

Yeast septin mislocalization to the plasma membrane

Keywords

Septins | yeast | plasma membrane | assembly

Acknowledgements

We thank Amy Gladfelter for advice on curvature measurement, Jeremy Thorner for advice on the *mss4-102* and *gin4*Δ phenotypes and the idea of V_C interference with the Cdc3–Cdc12 NC interface, and Jeff Moore for use of the confocal microscope and assistance with FRAP. Servier and DBCLS created vector graphics that we downloaded from http://www.bioicons.com. This work was supported by funds from the National Science Foundation, grant number 1928900, and by the National Institute of General Medical Sciences of the National Institutes of Health, grant numbers R01GM035010 and R35GM148198.

Conflict of interest statement

The authors declare no conflicts of interest.

Author contribution statement

Michael McMurray conceived and supervised this study. Aleyna Benson and Michael McMurray designed the experiments, and Aleyna Benson performed the experiments. Aleyna Benson and Michael McMurray performed data analysis, and took part in the interpretation of results and preparation of materials for the manuscript. Michael McMurray wrote the manuscript with comments from Aleyna Benson.

Data availability statement

Any raw data not already included in the main or supplementary material are available from the corresponding author upon reasonable request.

Abbreviations

AH amphipathic helix

BiFC bimolecular fluorescence complementation

DMSO dimethyl sulfoxide
ER endoplasmic reticulum

FCF forchlorfenuron

FRAP fluorescence recovery after photobleaching

GFP green fluorescent protein
GdnHCl guanidine hydrochloride
NTE N-terminal extension
PGAL GAL1/10 promoter

PI(4,5)P₂ phosphatidylinositol 4,5-bisphosphate

PLCδ phospholipase C delta

T-SNARE Target Soluble NSF (N-ethylmaleimide-sensitive factor) Attachment

Protein Receptor

V_N N-terminal Venus fragment V_C C-terminal Venus fragment YFP vellow fluorescent protein

ABSTRACT

Septin proteins contribute to many eukaryotic processes involving cellular membranes. In the budding yeast *Saccharomyces cerevisiae*, septin hetero-oligomers interact with the plasma membrane (PM) almost exclusively at the future site of cytokinesis. While multiple mechanisms of membrane recruitment have been identified, including direct

interactions with specific phospholipids and curvature-sensitive interactions via amphipathic helices, these do not fully explain why yeast septins do not localize all over the inner leaflet of the PM. While engineering an inducible split-YFP system to measure the kinetics of yeast septin complex assembly, we found that ectopic co-overexpression of two tagged septins, Cdc3 and Cdc10, resulted in nearly uniform PM localization, as well as perturbation of endogenous septin function. Septin localization and function in gametogenesis was also perturbed. PM localization required the C-terminal YFP fragment fused to the C terminus of Cdc3, the septin-associated kinases Cla4 and Gin4, and phosphotidylinositol-4,5-bis-phosphate (Pl(4,5)P₂), but not the putative Pl(4,5)P₂-binding residues in Cdc3. Endogenous Cdc10 was recruited to the PM, likely contributing to the functional interference. PM-localized septins did not exchange with the cytosolic pool, indicative of stable polymers. These findings provide new clues as to what normally restricts septin localization to specific membranes.

INTRODUCTION

Septin proteins interact with a wide variety of cellular membranes. Septins localize to specific regions of the inner face of the PM, including ER-PM junctions (Sharma et al., 2013); the outer mitochondrial membrane (Pagliuso et al., 2016); macropinosomes (Dolat and Spiliotis, 2016); synaptic vesicles (Beites et al., 1999); autophagosomes (Tóth et al., 2022) or pre-autophagosomal structures (Barve et al., 2018) and, in *Saccharomyces cerevisiae*, specific regions of the growing membrane that forms *de novo* around nascent gametes, called the prospore membrane (Fares et al., 1996). The mechanisms directing binding to specific membranes are incompletely understood.

Septins bind specific phospholipids via patches of positively-charged amino acids called "polybasic regions" (Zhang et al., 1999; Casamayor and Snyder, 2003), although it is unclear whether these polybasic regions are available for membrane interaction in the context of a septin filament (Jiao et al., 2020; Mendonça et al., 2021). For the five septins co-expressed in mitotically proliferating yeast cells (Cdc3, Cdc10, Cdc11, Cdc12 and Shs1), phosphotidylinositol-4,5-bis-phosphate (PI(4,5)P₂) plays a particularly important role in recruiting and maintaining septins as ring-shaped arrays of filaments at the regions of the PM where bud emergence and cytokinesis take place. Indeed,

PI(4,5)P₂ is enriched at the site of bud emergence and, later, at the bud neck (Garrenton et al., 2010). Depletion of yeast PI(4,5)P₂ leads to septin mislocalization (Rodríguez-Escudero et al., 2005; Bertin et al., 2010).

Additionally, yeast septin complexes exhibit a preference for membrane bilayers with a specific range of curvatures dictated by amphipathic helices (AHs) in Cdc12 and Shs1 (Cannon et al., 2019; Woods et al., 2021). Yeast septin filaments also organize in different orientations on lipid bilayers of different curvatures (Beber et al., 2019), which may explain changes in filament orientation seen in vivo during the PM remodeling at the bud neck that accompanies cytokinesis (McQuilken et al., 2017; DeMay et al., 2011; Vrabioiu and Mitchison, 2006; Ong et al., 2014). Ultimately, membrane curvature preference by septins is complex, involving multiple scales and assembly steps (Shi et al., 2023), and the minimal "rules" governing septin localization to a specific cellular membrane remain unclear.

We previously established a plasmid-based system for assessing the rate of *de novo* yeast septin folding and oligomerization that relies on the transcriptional induction of a single GFP-tagged septin using the GAL1/10 promoter (" P_{GAL} ") (Schaefer et al., 2016). Quantification of septin ring fluorescence is used as a proxy for successful incorporation of the GFP-tagged septin into polymerization-competent hetero-oligomers, whereas signal in the cytoplasm and nucleus is interpreted as representing septin-GFP molecules that have not yet incorporated into hetero-oligomers plus those that did achieve native assembly but did not polymerize into filaments. By measuring the kinetics of accumulation of septin ring signal relative to cytoplasm/nucleus signal at time points following the addition of galactose, we successfully applied this technique to identify both septin mutations (Schaefer et al., 2016) and chaperone mutations (Hassell et al., 2022) that slow septin folding/assembly. Here we sought to streamline this assay by eliminating the need to determine the subcellular localization of fluorescence signal. We previously used bimolecular fluorescence complementation (BiFC) to visualize septin-septin interactions in living cells, wherein one septin is fused to the N-terminal fragment of the YFP derivative Venus ("V_N") and another septin is fused to the smaller

Venus C-terminal fragment ("Vc") (Weems and McMurray, 2017). Fluorescence is observed only when the two septins physically interact, which requires successful *de novo* folding by both septins. Here we describe a single-plasmid approach to simultaneously co-overexpress two BiFC-tagged septins, Cdc3 and Cdc10, which unexpectedly resulted in interference with endogenous septin function and a change in septin membrane localization. These findings provide new insights into the mechanisms of septin complex assembly and membrane interactions.

MATERIALS AND METHODS

Yeast strains and plasmids

The following *S. cerevisiae* strains were cultured using standard techniques (Amberg et al., 2005). JTY3992 (CDC10-mCherry::kanMX (McMurray et al., 2011)), H06796 (CDC12-GFP::HIS3MX (Huh et al., 2003)), CBY06598 (mss4-102::kanMX (Li et al., 2011)), H06426 (swe1Δ::kanMX (Winzeler et al., 1999)), H07176 (cla4Δ::kanMX (Winzeler et al., 1999)), H06948 (*elm1*∆::*kanMX* (Winzeler et al., 1999)), H07177 $(gic2\Delta::kanMX \text{ (Winzeler et al., 1999)}), H06949 (gin4\Delta::kanMX \text{ (Winzeler et al., 1999)}),$ and H07178 (syp1∆::kanMX (Winzeler et al., 1999)) are derived from BY4741 (MATa $his3\Delta1 leu2\Delta0 met15\Delta0 ura3\Delta0$ (Winzeler et al., 1999)). JTY4024 (shs1 Δ ::kanMX (Winzeler et al., 1999)) is derived from BY4742 (MAT α his3 Δ 1 leu2 Δ 0 lys2 Δ 0 ura3 Δ 0) (Winzeler et al., 1999). M-1726 carries the *cdc12-6* mutation backcrossed extensively into the YEF473 background (Nagaraj et al., 2008). The $sfp1\Delta::kanMX/sfp1\Delta::kanMX$ strain H07150 (Winzeler et al., 1999) is derived from BY4743 (MATa/MATa $his3\Delta1/his3\Delta1$ $leu2\Delta0/leu2\Delta0$ $lys2\Delta0/LYS2$ $met15\Delta0/MET15$ $ura3\Delta0/ura3\Delta0$ (Winzeler et al., 1999)). YEF5690 is in the YEF473 background and carries CDC10-V_N::kanMX (Oh et al., 2013). H07151 was made by integrating mCherry-CDC3::LEU2 at the CDC3 locus of BY4741 using Bg/II-cut Yip128-Cdc3-mCherry (Wloka et al., 2011). MMY0265 was made by mating FY2742 with FY2839, which are $his3\Delta 1 leu2\Delta 0 lys2\Delta 0 ura3\Delta 0$ and MATa or $MAT\alpha$, respectively, with polymorphisms in three genes from the SK1 background (MKT1(G30) RME1 TAO3(Q1493)) that increase sporulation efficiency (Kloimwieder and Winston, 2011). The Gal4-estrogen binding domain-VP16 fusion

protein was integrated at the genomic $leu2\Delta 0$ allele of MMY0265 using Pmel-cut plasmid pAGL, creating strain H07172.

Plasmids are described in Table S1. Plasmids were introduced using the Frozen-EZ Yeast Transformation II Kit (#T2001, Zymo Research). Cells were cultured in liquid or solid (2% agar) rich (1% yeast extract, 2% peptone, 2% glucose), synthetic medium (SC; per liter, 20 g glucose or lactose, 1.7 g yeast nitrogen base without amino acids or ammonium sulfate, 5 g ammonium sulfate, 0.05 g tyrosine, 0.01 g arginine, 0.05 g aspartate, 0.05 g phenylalanine, 0.05 g proline, 0.05 g serine, 0.1 g threonine, 0.05 g valine, 0.05 g histidine, 0.1 g uracil, and 0.1 g leucine), or sporulation medium (1% potassium acetate, 0.05% glucose, 20 mg/L leucine, 40 mg/L uracil). Where appropriate to maintain plasmid selection, synthetic medium lacked specific components (uracil and/or leucine). FCF (Santa Cruz Biotechnology #sc-204759) was dissolved in DMSO to make a 1 M stock. Guanidine hydrochloride (Research Products International #G49000) was dissolved in water to make a 5 M stock. β-estradiol (Sigma-Aldrich #E2758) was dissolved in 100% ethanol to make a 5 mM stock.

Microscopy

Most images were captured with an EVOSfl all-in-one epifluorescence microscope (Thermo-Fisher Scientific) with a 60× oil objective and GFP (#AMEP4651), CFP (#AMEP-4653) and Texas Red (#AMEP4655) LED/filter cubes. Image adjustment and analysis was carried out using FIJI software (Schindelin et al., 2012). All images of the same type were analyzed in the same way. For analysis of folding/assembly kinetics, 3-mL cultures were grown overnight in synthetic medium lacking uracil and containing 2% lactose to mid-log phase prior to induction. Aliquots were taken at timepoints and spotted on 1% agarose pads then covered with an 18 mm x 18 mm coverslip (#1.5) for imaging. Cellular fluorescence captured with the GFP LED cube at 80% intensity and 250-msec exposures was quantified by drawing an 8-pixel-wide line across the middle of each cell and using the "Plot profile" command in FIJI. Each cell was assigned a single value corresponding to the maximum value along the profile. Identities of images for quantification were blinded prior to analysis to prevent bias.

Cell length:width ratios were calculated in FIJI by measuring the length of lines drawn from one end of a cell to another along the long (length) or short (width) axis, with an obvious constriction representing a boundary between cells. The length:width ratio was calculated for each of 100 cells and then the percentage of cells with length:width > 2 was determined. The Fisher's Exact test (two-tailed) was applied using a 2x2 contingency table in GraphPad Prism to determine P values for the differences in the percentage of elongated cells, comparing one sample against a reference. These quantifications were not performed blind.

For FRAP, images were collected on a spinning disk confocal Nikon Ti-E microscope equipped with a 1.45 NA 100× CFI Plan Apo objective, piezo electric stage (Physik Instrumente; Auburn, MA), spinning disk confocal scanner unit (CSU10; Yokogawa), 488-nm laser (Agilent Technologies; Santa Clara, CA), TI-LA FRAP module, and an EMCCD camera (iXon Ultra 897; Andor Technology; Belfast, UK) using NIS Elements software (Nikon). Single z-plane images were collected at 10sec intervals, with the 488-nm laser at 70% power and a 100-msec exposure. For each photobleaching experiment, we first collected a 'pre-bleached' images, then a region of the cell cortex was bleached for 400msec with the 488-nm laser at 100% power. For analysis, a circular ~0.015 µm² region of interest was selected in the bleached area and the average intensity was recorded over 910 sec. A separate region of equal size was drawn in an unbleached region of the cell cortex and the average intensity was recorded over the same time period.

AlphaFold2 Multimer structure prediction

We used ColabFold v1.5.2: AlphaFold2 using MMseqs2 (Mirdita et al., 2022), at https://colab.research.google.com/github/sokrypton/ColabFold/blob/main/AlphaFold2.ipy ip using the default settings (which use AlphaFold2 Multimer v3) and the full predicted amino acid sequence of Cdc3 and Cdc10. Output models in .pdb format were rendered in PyMOL (Schrödinger, LLC).

RESULTS

Localization-independent assay of in vivo septin folding/assembly kinetics

 P_{GAL} is bi-directional, driving transcription of both the GAL1 and GAL10 genes that flank it (Elison et al., 2018). Cdc3 and Cdc10 directly interact within septin hetero-octamers, which are linear complexes of the order Cdc11/Shs1-Cdc12-Cdc3-Cdc10-Cdc10-Cdc3-Cdc12-Cdc11/Shs1 (Bertin et al., 2008). We engineered a low-copy plasmid in which transcription of both CDC3- V_C and CDC10- V_N are under control of the same P_{GAL} sequence, and expression is induced by addition of galactose to the growth medium. Since many C-terminal tags are known to compromise septin function in a manner often exacerbated by high temperature (McMurray, 2016), we cultured cells at room temperature (~22°C). We quantified total cellular fluorescence in wild-type haploid cells at time points following induction and observed a gradual increase in signal, indicative of transcription, translation, folding and assembly of the tagged Cdc3 and Cdc10, and reconstitution and maturation of the split fluorophore (Figure 1A,B). The kinetics of accumulation (<2-fold over 7 hr) were considerably slower than for GFP-tagged Cdc3, for which fluorescence increased >4-fold in 6 hr, even though here we used a higher concentration of galactose (Schaefer et al., 2016; Hassell et al., 2022).

To assess the impact of slowing septin folding, we introduced the G365R mutation into Cdc3-Vc. Gly365 lies within a key part of the Cdc3–Cdc10 interface (Weems et al., 2014). We previously used P_{GAL} coupled with a GFP tag to show that at temperatures permissive for proliferation, the G365R mutation slows ~2-fold Cdc3 folding and/or assembly into septin hetero-oligomers (Schaefer et al., 2016). BiFC fluorescence was consistently lower for the G365R mutant, but it accumulated at approximately the same rate as wild-type Cdc3-Vc (Figure 1B). Thus BiFC signal is consistent with assembly of Cdc3–Cdc10 heterodimers involving Gly365 but this assay is not particularly sensitive to changes in septin folding.

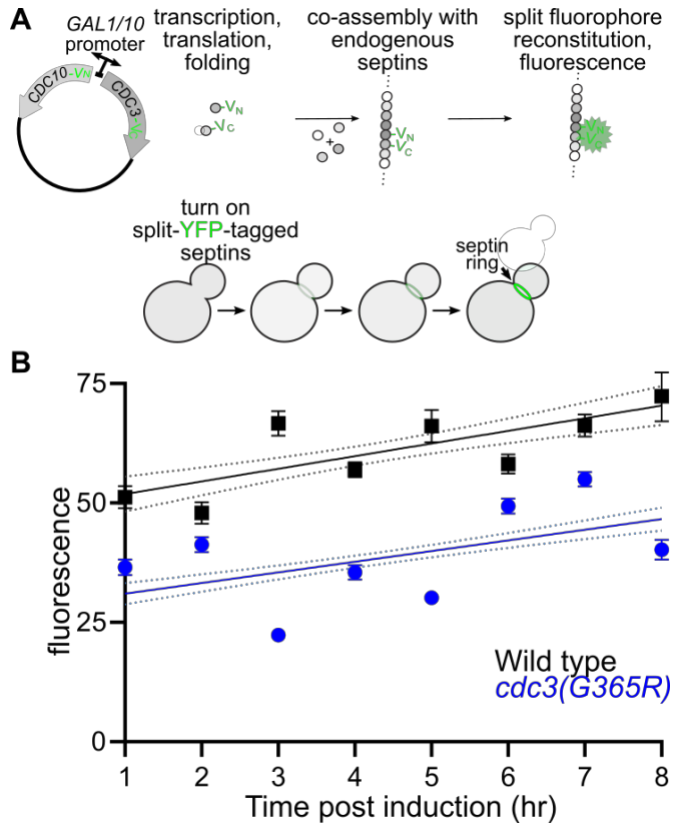


Figure 1. Slow kinetics of fluorescence accumulation following induction of co-expression of BiFC-tagged Cdc3 and Cdc10. (A) Schematic illustration of the experimental plan. A single plasmid encodes BiFC-tagged Cdc3 and Cdc10 under control of the bidirectional *GAL1/10* promoter. Addition of galactose turns on tagged septin expression. Once translated and folded, the tagged septins co-assemble with endogenous septins into septin hetero-octamers that polymerize into filaments at the septin ring at the yeast bud neck. Reconstitution of the split fluorophore generates fluorescence signal. Fluorescence quantification over time reveals the kinetics of septin transcription. (B) For cells (strain BY4741) carrying plasmid pPgal-Cdc3-Vc—Cdc10-Vn ("Wild type") or the *cdc3(G365R)* derivative G00823 ("*cdc3(G365R)*"), cellular fluorescence (mean ± standard error of the mean) was measured by microscopy for ≥50 cells per timepoint, after the indicated interval following addition of galactose to final concentration 2%. Lines represent best-fit linear regression with 95% confidence intervals (dashed lines).

Aberrant plasma membrane localization of BiFC signal

Individual overexpression of tagged wild-type Cdc3 or Cdc10 results in septin ring signal plus accumulation diffusely throughout the cytoplasm/nucleus (Johnson et al., 2015; Hassell et al., 2022). Unexpectedly, and especially after long induction times, BiFC signal was often found extensively along the PM (Figure 2A). Some cells also had roundish internal signals that resembled nuclei (see arrowheads in Figure 2A); we did not further study these signals. Cells with strong PM signal were also frequently elongated and had multiple buds attached to the same mother cell, regardless of incubation temperature (Figure 2A, Table 1). The presence of multiple elongated buds

is a distinctive feature of septin dysfunction (Hartwell, 1971). Defects in septin ring assembly prolong isotropic bud growth and cause elongated bud morphologies via a Swe1-dependent G₂/M delay known as the morphogenesis checkpoint (Barral et al., 1999; Shulewitz et al., 1999; Longtine et al., 2000; Lew, 2003). Only individual overexpression of Cdc11 or Shs1 perturbs septin function in otherwise wild-type cells (Sopko et al., 2006). Hence these observations pointed to novel properties of the co-overexpressed Cdc3 and Cdc10.

We saw no PM mislocalization or dominant-negative functional effects in previous studies with these same BiFC-tagged versions of Cdc3 and Cdc10 (Garcia et al., 2016; Weems and McMurray, 2017; Denney et al., 2021), but in those studies the tagged septins were expressed at endogenous levels from the native promoters. We systematically manipulated individual features of the BiFC co-overexpression construct to determine which were necessary and/or sufficient for PM mislocalization and perturbation of septin function. First, we made an improved version of the plasmid. The way we constructed the original version resulted in an unnecessarily large plasmid (16 kb) with multiple repeated sequences (Figure S1A). In multiple cases, yeast or bacterial transformants appeared to carry smaller versions of the plasmid that had lost the septin genes (data not shown), presumably due to recombination between the repeated sequences. To avoid this problem, we created a "streamlined" plasmid about half the size with no sequence repeats (Figure S1A), which caused elongated bud morphologies that were more penetrant than the original, recombination-prone plasmid (Figure S1B, Table 1). We quantified cell elongation by calculating the length:width ratio for 100 cells per genotype (Figure 2B, Figure S2, Table 1). To summarize the results of our manipulations: we found that PM localization and severe perturbation of endogenous septin function required co-overexpression and, surprisingly, the V_C tag fused to the C terminus of Cdc3. Overexpression of Cdc3-V_c alone in cells expressing Cdc10-V_N at endogenous levels resulted only in BiFC signal to normal septin rings (Figure 2C). When Cdc3-V_C and tagged Cdc10 were co-overexpressed from the same P_{GAL} on the same plasmid, fluorescence intensity varied from cell to cell but PM localization was observed in nearly every cell that exhibited fluorescence (Figure 2A,D, Table 1),

whereas when they were encoded on different plasmids, many cells instead had diffuse cytoplasmic/nuclear signal (Figure 2E, Table 1). As expected, the elongated morphologies reflect activation of the morphogenesis checkpoint: $swe1\Delta$ cells co-overexpressing Cdc3-V_C and Cdc10-V_N were much rounder than $SWE1^+$ cells, despite persistent PM localization of the BiFC signal (Figure 2F, Table 1).

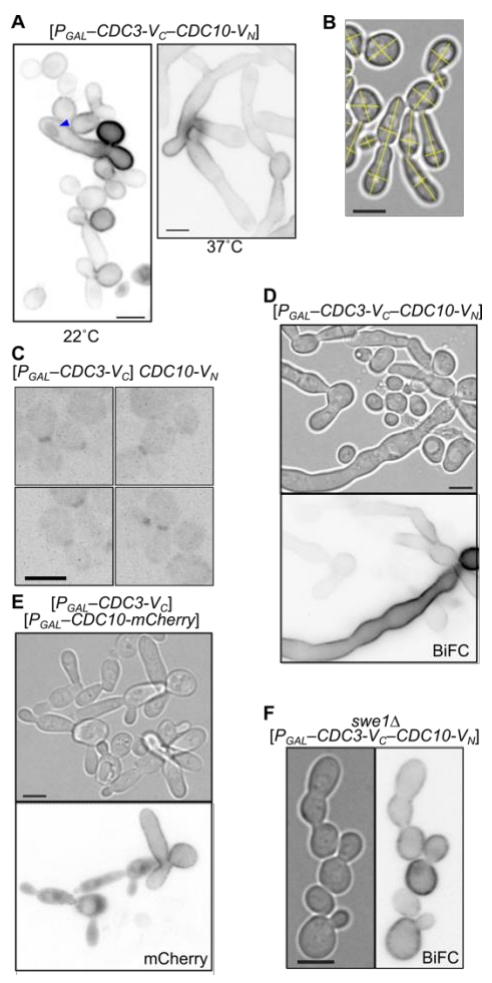


Figure 2. Plasma membrane mislocalization of co-overexpressed Cdc3-V_C and Cdc10. Haploid cells of the indicated genotype were imaged with transmitted light or for reconstituted YFP (BiFC) or mCherry fluorescence, as indicated. Brackets denote genes encoded on plasmids. All cells were imaged following overnight culture at 22°C (A-C) or 30°C (D-E) in plasmid-selective liquid medium with 2% galactose. Fluorescence images were inverted for clarity. Scale bars, 5 μm. (A) Strain BY4741 with plasmid G00805. GFP LED cube, 100% intensity 250-msec exposure. (B) Strain BY4741 with plasmids pMVB1 and G00526, showing lines drawn in FIJI to calculate length:width ratio. (C) Strain YEF5690 with plasmid pPgal-Cdc3-Vc. GFP LED cube, 90% intensity, 500-msec exposure. (D) Strain BY4741 with plasmid E00432. GFP LED cube, 100% intensity, 120-msec exposure. (E) Strain BY4741 with plasmids G00545 and G00526. Texas Red LED cube, 100% intensity, 250-msec exposure. (F) Strain H06426 with plasmid E00432. GFP LED cube, 100% intensity, 250-msec exposure.

Plasma membrane mislocalization of endogenous Cdc10 by co-overexpression of BiFC-tagged Cdc3 and Cdc10

Septin dysfunction upon co-overexpression of BiFC-tagged Cdc3 and Cdc10 could result from mislocalization of the endogenously expressed septins to the PM away from the bud neck, sequestering septin subunits required for normal septin ring assembly. We monitored the localization of endogenous septins fluorescently tagged at their chromosomal loci or expressed from low-copy plasmids from native promoters in cells co-overexpressing Vc-tagged Cdc3 and Cdc10 from the same promoter and plasmid.

Whereas in cells with an empty vector, endogenous Cdc10-mCherry localized mostly to bud necks (and faintly in the cytoplasm/nucleus), in cells with the septin co-expression plasmid endogenous Cdc10-mCherry localized all around the PM in elongated cells (Figure 3A,B). By contrast, endogenous mCherry-tagged Cdc3 was not recruited to the PM (Figure 3C). When we introduced the V_N-less version of the co-overexpression plasmid into cells with GFP-tagged endogenous Cdc12 or a plasmid encoding YFPtagged Cdc11 or GFP-tagged Shs1, we saw no mislocalization of Cdc12-GFP, Cdc11-YFP, or Shs1-GFP to the PM (Figure 3D-I). Occasional ectopic assemblies containing Cdc12-GFP or Shs1-GFP are artifacts of the GFP tags and were also present in cells not co-overexpressing Cdc3-Vc and Cdc10 (Figure 3E,H). Upon co-overexpression of Cdc3-V_C and untagged Cdc10, the Shs1-GFP-expressing cells were much less elongated than cells without the tagged Shs1 (Figure 31, Table 1). We confirmed that the co-overexpressed septins still localized to the PM in Shs1-GFP-expressing cells by using the plasmid with both BiFC tags (Figure 3J). P_{GAL} induction may have been weaker in this experiment, leading to rounder cells and dimmer PM signal. We conclude that the co-overexpressed Cdc3-V_C and Cdc10 drive PM mislocalization of endogenous Cdc10 but not Cdc3, Cdc11, Cdc12 or Shs1.

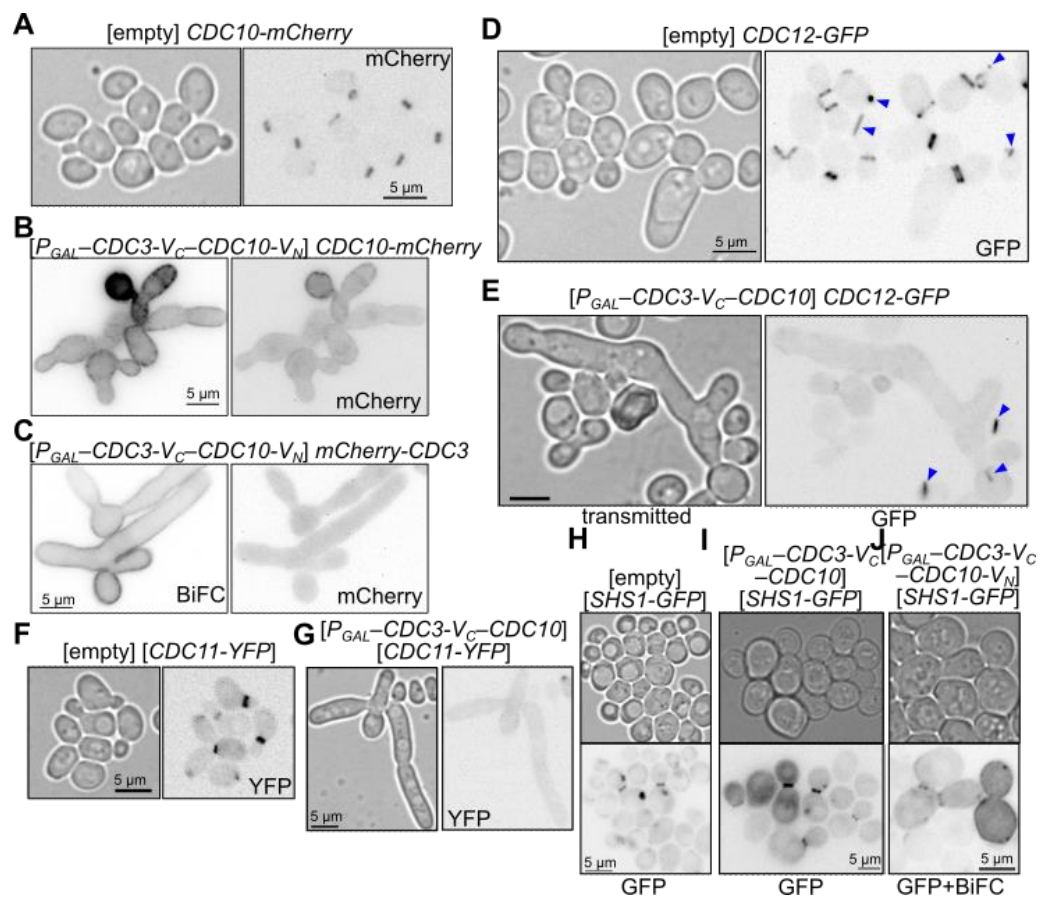


Figure 3. Co-overexpressed Cdc3 and Cdc10 drive plasma membrane mislocalization specifically of endogenous Cdc10. Haploid cells of the indicated genotype were imaged with transmitted light or for GFP, YFP, or mCherry fluorescence. All cells were imaged following overnight culture in plasmid-selective liquid medium with 2% galactose. Images were inverted for clarity. "BiFC" is YFP signal arising from Cdc3-V_C-Cdc10-V_N interaction. Brackets denote genes encoded on plasmids, otherwise genotypes reflect the alleles the chromosomal loci. (A) Strain JTY3992 (CDC10-mCherry) with plasmid pRS316. Texas Red LED cube 100% intensity, 1 sec exposure. (B) Strain JTY3992 with plasmid E00432. Texas Red LED cube 100% intensity, 1.5 sec exposure. (C) H07151 with plasmid E00432. GFP LED cube 60% intensity, 120-msec exposure; Texas Red LED cube 100% intensity, 1.5 sec exposure. (D) Strain H06796 with plasmid pRS316, GFP LED cube 100% intensity, 500-msec exposure. Blue arrowheads point to ectopic septin structures that are commonly found in this Cdc12-GFP and are an artifact of the GFP tag. (E) Strain H06796 with plasmid E00431, GFP LED cube 100% intensity, 500-msec exposure. (F) Strain BY4741 with plasmids pML43 and pRS316, GFP filter 100% intensity, 500-msec exposure. (G) Strain BY4741 with plasmids pML43 and E00431, GFP filter 100% intensity, 750-msec exposure. (H-I) Strain BY4741 with plasmids pRS315-SHS1-GFP and pRS316 ("empty") and E00431, GFP filter 100% intensity, 250-msec exposure, (J) BY4741 with plasmids pRS315-SHS1-GFP and E00432, GFP filter 100% intensity,120-msec exposure.

Requirement for Cla4 and Gin4, but not Elm1, Gic2, or Syp1, in PM mislocalization

A number of non-septin proteins are important in proper septin localization. In cells lacking the kinase Cla4, which directly phosphorylates both Cdc3 and Cdc10, septins mislocalize along extensive regions of the bud PM (Versele and Thorner, 2004; Schmidt

et al., 2003; Cvrcková et al., 1995). The kinase Gin4 phosphorylates Shs1 (Asano et al., 2006) and septin localization in *gin4* mutants is often aberrant (Longtine et al., 1998). Elm1 phosphorylates the septin-binding protein Bni5 and regulates septin filament pairing and localization (Patasi et al., 2015; Bouquin et al., 2000; Marguardt et al., 2020). The paralogous Cdc42 effector proteins Gic1 and Gic2 have been implicated in septin recruitment (Iwase et al., 2006) and Gic1 interacts directly with Cdc10 in the context of septin hetero-octamers and filaments (Sadian et al., 2013). Syp1 directly bundles septin filaments and regulates septin ring assembly in vivo (Ibanes et al., 2022). We introduced the streamlined Cdc3- and Cdc10-co-overexpressing plasmid into haploid cells carrying deletion alleles of CLA4, GIN4, ELM1, GIC2, or SYP1 and monitored BiFC signal localization and bud morphology. Only $cla4\Delta$ and $gin4\Delta$ blocked PM localization, and both of these mutations also drastically reduced bud elongation, to extents similar to that of swe 1Δ (Figure 4A, Table 1). Mating $cla4\Delta$ or $gin4\Delta$ cells carrying the co-overexpression plasmid with a wild-type haploid strain restored PM localization in the diploid cells (Figure 4A), consistent with the defects being recessive phenotypes of the deletion alleles.

The synthetic plant cytokinin forchlorfenuron (FCF) perturbs septin localization in most cell types, including *S. cerevisiae* (Iwase et al., 2004), via an unknown mechanism. We asked if the PM localization of co-overexpressed Cdc3 and Cdc10 is sensitive to FCF. Endogenously mCherry-tagged Cdc10 showed the expected ectopic mislocalization patterns ("bars", puncta) upon overnight exposure to 1 mM FCF, but the PM BiFC localization was unaffected (Figure 4B). Thus the PM-localized septin complexes appear to be insensitive to perturbation by FCF. Together, these data suggest that the PM-associated complexes have distinct requirements for membrane association compared to native septins.

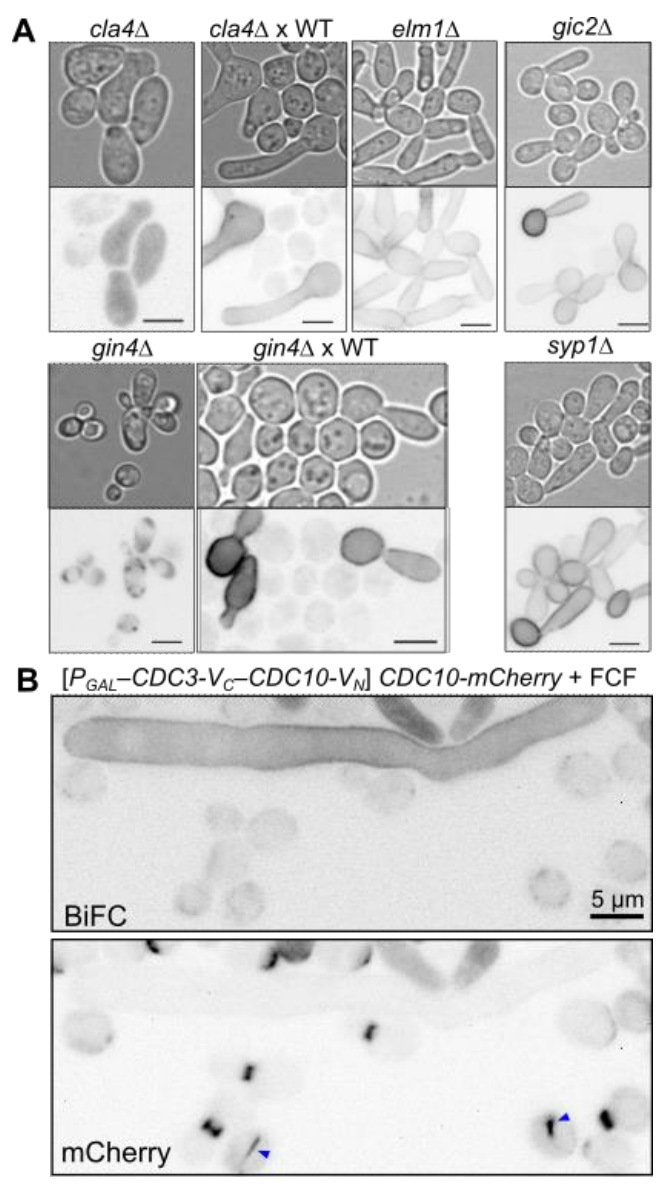


Figure 4. Loss of septin mislocalization to the plasma membrane in cells lacking Cla4 or Gin4. All cells were imaged following overnight culture in plasmid-selective liquid medium with 2% galactose. Images were inverted for clarity. (A) The indicated mutant derivatives of haploid strain BY4741 carrying plasmid E00432. Where indicated ("x WT"), the mutant haploids were mixed with haploid cells of the opposite mating type (strain BY4742) to allow mating and provide a wild-type copy of the deleted gene. GFP LED cube 100% intensity, 500-msec exposure for $cla4\Delta$, $gin4\Delta$ and ("x WT"). GFP LED cube 100% intensity, 120-msec exposure for $elm1\Delta$, $gic2\Delta$, and $syp1\Delta$. (B) Strain JTY3992 with plasmid E00432 cultured in the presence of 1 mM FCF. GFP LED cube 80% intensity, 250-msec exposure; Texas Red LED cube 100% intensity, 1.5-sec exposure. Blue arrowheads point to ectopic septin structures induced by FCF. Scale bars, 5 µm.

Lack of membrane curvature preference in aberrant septin localization following co-overexpression of Cdc3 and Cdc10

The elongated cells produced upon co-overexpression of BiFC-tagged Cdc3 and Cdc10 provided a range of PM curvatures, allowing us to ask if the intensity of BiFC signal correlated with apparent PM curvature. We assumed roughly cylindrical 3D shapes of elongated cells and roughly spherical shapes of round cells, and estimated PM curvature using 2D images and the Kappa plugin in ImageJ. In cells with round buds, septin filaments are found only at the bud neck, the site of the most curved regions of the PM, and our analysis recapitulated this result with Cdc12-GFP (Figure 5A). However, just because the yeast bud neck has the regions of highest PM curvature does not mean that yeast septins localize to all highly curved regions of the PM. Indeed, we could find examples of misshapen cells co-expressing BiFC-tagged Cdc3 and Cdc10 in which fluorescence was found exclusively at the bud neck but not elsewhere at the PM, including at regions of similar curvature away from the neck (Figure 5B, see blue arrowheads). [Note that the unusual but informative cell shown in Figure 5B is from a culture of diploid cells in which the gene SFP1 was deleted; diploid cells lacking Sfp1 are smaller than wild-type cells (Ni and Snyder, 2001). The impetus for this experiment was a misleading observation in which wild-type diploid cells appeared to lack PM BiFC localization, so we used the SFP1 deletion to ask if larger cell size in diploids was responsible for this apparent difference. However, the loss of PM signal in wild-type diploids was not seen in other experiments with the original BiFC plasmid or with the "streamlined" BiFC plasmid, hence we attribute the original observation to recombination that eliminated the septin genes.]

The same kind of analysis revealed that while BiFC signal at the PM away from the bud neck varied in intensity along the PM, there was no clear correlation with membrane curvature (Figure 5C-E). While we cannot exclude the possibility that our single-focal-plane images failed to capture more complex 3D PM contours with different curvatures in dimensions other than *x-y*, we interpret these data as evidence that the septin PM localization in cells co-overexpressing Vc-tagged Cdc3 and Cdc10 is largely independent of PM curvature. Since new PM synthesis occurs mostly in the bud as it grows, if the Cdc3–Cdc10 complexes bind the PM as soon as they are able, then signal

variation along the PM may reflect the level of co-overexpression at the time when that part of the bud PM was being synthesized.

AHs in the yeast septins Cdc12 (Cannon et al., 2019) and Shs1 (Woods et al., 2021) are sufficient to impart curvature preference in vitro, and mutating the Cdc12 AH eliminates curvature preference of complexes containing Cdc11 (which has no AH) in place of Shs1 (Cannon et al., 2019). The PM localization of BiFC signal arising from cooverexpressed Cdc3-V_C and Cdc10-V_N did not appear to require a fully-functional AH from Cdc12 or Shs1, because PM localization was observed in cells carrying either an allele of CDC12 that truncates most of the helix (cdc12-6 (Cannon et al., 2019)) or a deletion allele of SHS1 (Figure 5F). For endogenous, wild-type septins, shifting cdc12-6 cells to high temperature (37°C) triggers rapid (within 30 minutes (Kim et al., 1991; Barral et al., 2000) loss of membrane (bud neck) localization, but BiFC signal at the PM persisted for hours after incubation at 37°C (Figure 5F). We note that at 37°C *cdc12-6* cells eventually become elongated (Kim et al., 1991), but elongation requires cell growth and growth in synthetic galactose medium is quite slow. In fact, in *cdc12-6* cells at 22°C the elongated bud phenotype resulting from co-overexpression was much less severe than in wild-type cells (Figure 5F, Table 1), but we cannot exclude that this simply reflects lower levels of co-overexpression in this genetic background. Complete deletion of the Cdc12 helix is lethal (Woods et al., 2021) as is combining the *cdc12-6* and *shs1*\Delta alleles (Finnigan et al., 2015), hence we could not test the effects on the absence of both helices on septin PM localization.

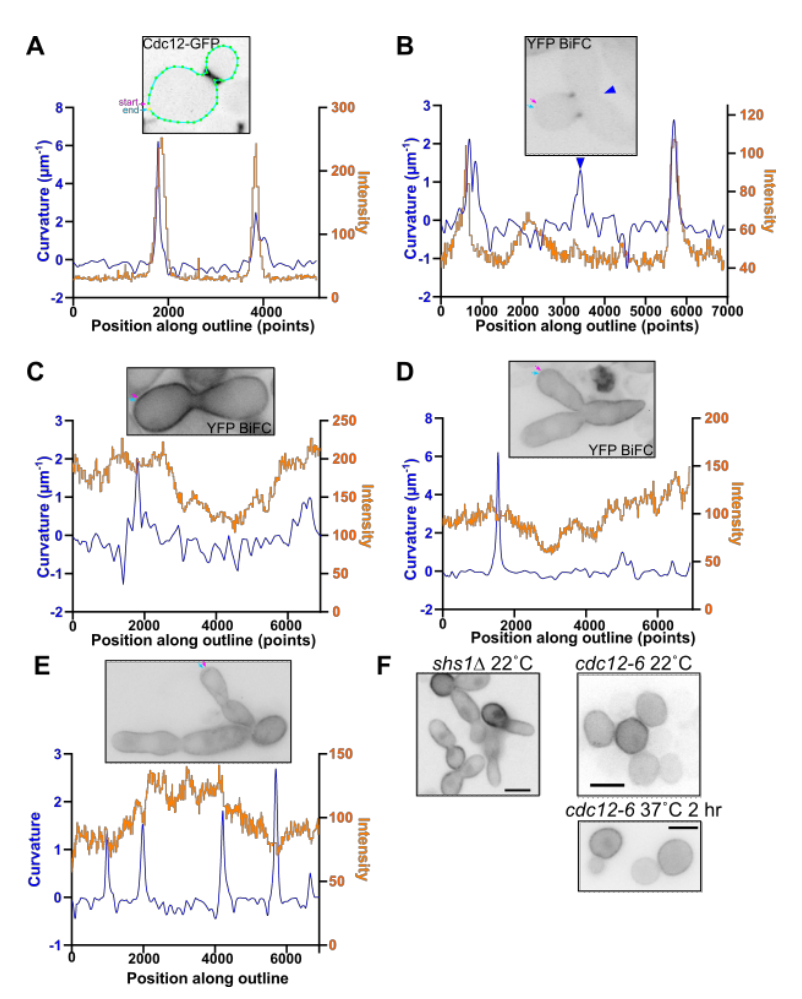


Figure 5. Plasma membrane mislocalization of co-overexpressed Cdc3 and Cdc10 is largely independent of membrane curvature and does not require the amphipathic helix of Cdc12 or **Shs1.** All cells were imaged following overnight culture in plasmid-selective liquid medium with 2% galactose. Images were inverted for clarity. (A-E) PM curvature was estimated from 2D fluorescent micrographs of yeast cells (inset above) using the Kappa plugin for ImageJ. Plots show local curvature and fluorescence intensity at each point along the trace of the plasma membrane (cell outline). (A) Cdc12-GFP in haploid cells of strain H06796 carrying the empty vector plasmid pRS316. GFP LED cube 100% intensity, 500-msec exposure. The cyan line with green points indicates the cell outline used for measurement. Yellow point marks the end of the outline. (B) BiFC signal in $sfp1\Delta/sfp1\Delta$ diploid cells (strain H07150; note that deletion of SFP1 is likely irrelevant to the phenotype) resulting from interaction of Cdc3-V_C and Cdc10-V_N co-expressed from plasmid E00432. GFP LED cube 100% intensity, 250-msec exposure. This cell, with an unusual shape and some fluorescence at the bud neck, was not representative of most cells in the culture. (C-E) As in (B) but with wild-type diploid cells (BY4743). GFP LED cube 100% intensity, 250-msec exposure. (F) Representative fluorescence micrographs of cells of the indicated genotype ("shs1\Delta", JTY4024; cdc12-6, M-1726) carrying plasmid G00865. CFP LED cube, 100% intensity, 250-msec exposure for shs1\(\Delta\), 60-msec exposure for cdc12-6. Where indicated, cells were incubated at 37°C for 2 hr. Scale bars, 5 µm.

Co-overexpression of Cdc3-V $_{\text{C}}$ and Cdc10 dominantly perturbs septin function in sporulation

Notably, the only case in wild-type *S. cerevisiae* cells in which septin complexes are normally found uniformly around the PM is at the late stages of sporulation, the process during yeast gametogenesis by which the haploid nuclei produced by meiosis are packaged into new membranes and cell walls (Fares et al., 1996; Pablo-Hernando et al., 2008). We induced co-overexpression of Cdc3-Vc and Cdc10-V_N in diploid cells induced to undergo sporulation and measured the "success" of sporulation by counting the number of spores produced per diploid cell. We previously showed that in septin mutants spore number is decreased, presumably because prospore membranes grow in the wrong directions without guidance from higher-order septin structures (Garcia et al., 2016; Heasley and McMurray, 2016). Sporulation is typically induced using medium lacking a nitrogen source and containing no or a low concentration of a non-fermentable carbon source. To induce P_{GAL} expression in sporulation medium without adding 2% galactose, we integrated a plasmid encoding a fusion of the Gal4 DNA-binding domain with the VP16 transcriptional activation domain and an estrogen binding domain, which allows induction of P_{GAL} expression via the addition of estradiol (Veatch et al., 2009).

Sporulation proceeded normally in the presence of Cdc3-GFP overexpression: after five days in sporulation medium, when we examined 70 diploid cells that initiated sporulation, 54 (77%) produced the maximum four spores ("tetrads"), and only one (1.4%) produced a "dyad" (two spores). By contrast, co-overexpression of Cdc3-Vc and Cdc10-V_N essentially inverted the frequencies of tetrads (1 of 70, 1.4%) and dyads (64 of 70, 91%). Cdc3-GFP signal was mostly in the residual cytoplasm trapped between the four spores, with some signal that appeared to be nuclear (Figure 6A). BiFC signal was mostly at spore PMs, but in a more punctate pattern than what we saw in vegetatively proliferating cells (Figure 6A) or for normal septin localization in spores (Fares et al., 1996; Pablo-Hernando et al., 2008). Frequently, only one spore in a dyad had BiFC signal (Figure 6A), presumably reflecting random plasmid segregation during meiosis and synthesis of Cdc3-Vc and Cdc10-V_N after spore membranes closed. These data demonstrate perturbation of endogenous septin function in another context and that co-overexpressed Cdc3-V_C and Cdc10 also bind pervasively to the newly-formed PMs of spores.

Plasma membrane mislocalization of co-overexpressed Cdc3- V_{C} and Cdc10 requires phosphotidylinositol-4,5-bis-phosphate but not the polybasic regions in Cdc3

PI(4,5)P₂ is enriched at the bud neck but is present throughout the PM (Garrenton et al., 2010). Maintenance of PM PI(4,5)P₂ requires the kinase Mss4, and PI(4,5)P₂ is rapidly depleted from the PM when cells expressing a temperature-sensitive mutant (mss4-102) are shifted to 37°C (Stefan et al., 2002). GFP-tagged wild-type Cdc10 also disappears from the bud necks of mss4-102 cells at 37°C (Bertin et al., 2010). To ask if the aberrant PM localization of co-overexpressed, BiFC-tagged Cdc3 and Cdc10 requires PI(4,5)P₂, we transformed haploid mss4-102 cells with a P_{GAL} – $Cdc3-V_C$ – $Cdc10-V_N$ plasmid and localized BiFC signal following induction with galactose. To our surprise, there was no PM signal even at the temperature permissive for colony growth (22°C) (Figure 6B). Instead, BiFC signal was mostly diffuse in the cytoplasm/nucleus and excluded from vacuoles (Figure 6B). The cells were also round, indicating a lack of perturbation of septin function.

We introduced the same plasmid previously used by others to monitor PI(4,5)P₂ localization in *mss4-102* cells — a fusion of GFP with a tandemly repeated PH domain from human PLCδ (phospholipase C) (Stefan et al., 2002) — and also saw no PM signal (Figure 6C). When we mated the *mss4-102* cells carrying the PI(4,5)P₂ reporter plasmid to a wild-type haploid, restoring wild-type Mss4, we saw the expected PM signal (Figure 6D). To our knowledge, this is the first time this PI(4,5)P₂ reporter has been tested in cells in which the only source of Mss4 is the *mss4-102* allele present at the endogenous *MSS4* locus. The *mss4-102* allele was originally generated on a plasmid and characterized in cells carrying the plasmid and a deletion allele at the endogenous *MSS4* locus (Stefan et al., 2002), and other studies reporting PI(4,5)P₂ localization used the same "covering plasmid" approach (Garrenton et al., 2010). In studies of this (Stefan et al., 2002) and other temperature-sensitive *mss4* mutants (Desrivières et al., 1998; Homma et al., 1998), significant defects in PI(4,5)P₂ synthesis and/or associated phenotypes were reported at the temperature permissive for yeast

colony/culture growth. We interpret our data as evidence that: (i) at 22°C PI(4,5)P₂ levels at the PM in cells carrying the *mss4-102* allele at the *MSS4* chromosomal locus are too low to be detected with the GFP-2X-PH(PLCδ) reporter; (iii) plasmid-encoded *mss4-102* provides extra gene copies per cell that boost Mss4 protein levels and, consequently, activity at permissive temperatures; and (ii) the low PI(4,5)P₂ levels at the PM in chromosomal *mss4-102* cells do not support PM localization of co-overexpressed Cdc3 and Cdc10. Thus PM mislocalization of co-overexpressed Cdc3 and Cdc10 requires PI(4,5)P₂ at the PM, presumably via direct septin-phospholipid interaction.

The Cdc10 polybasic region is thought to be particularly important for $PI(4,5)P_2$ -mediated membrane interaction by septin hetero-octamers *in vitro* (Bertin et al., 2010). Because the Cdc10 polybasic region lies entirely within the $\alpha 0$ helix, which makes critical contacts across the NC interface, mutating those basic residues to Ala disrupts the NC interface and splits hetero-octamers into hetero-tetramers (Bertin et al., 2010). In an attempt to more specifically perturb $PI(4,5)P_2$ interactions by the co-overexpressed Cdc3–Cdc10 complex, we instead targeted the two polybasic regions in Cdc3. Mutating all the basic residues in both regions subtly perturbs filament assembly on synthetic membranes *in vitro* (Bertin et al., 2010). We deleted the N-terminal 100 residues, which includes Lys90, Arg93 and Arg94 plus the intrinsically disordered N-terminal extension (NTE) (Weems and McMurray, 2017), and additionally mutated Arg111, Arg112 and Lys115 to Ala. These mutations had no obvious effect (Figure S3, Table 1). Thus PM localization does not require the Cdc3 polybasic regions.

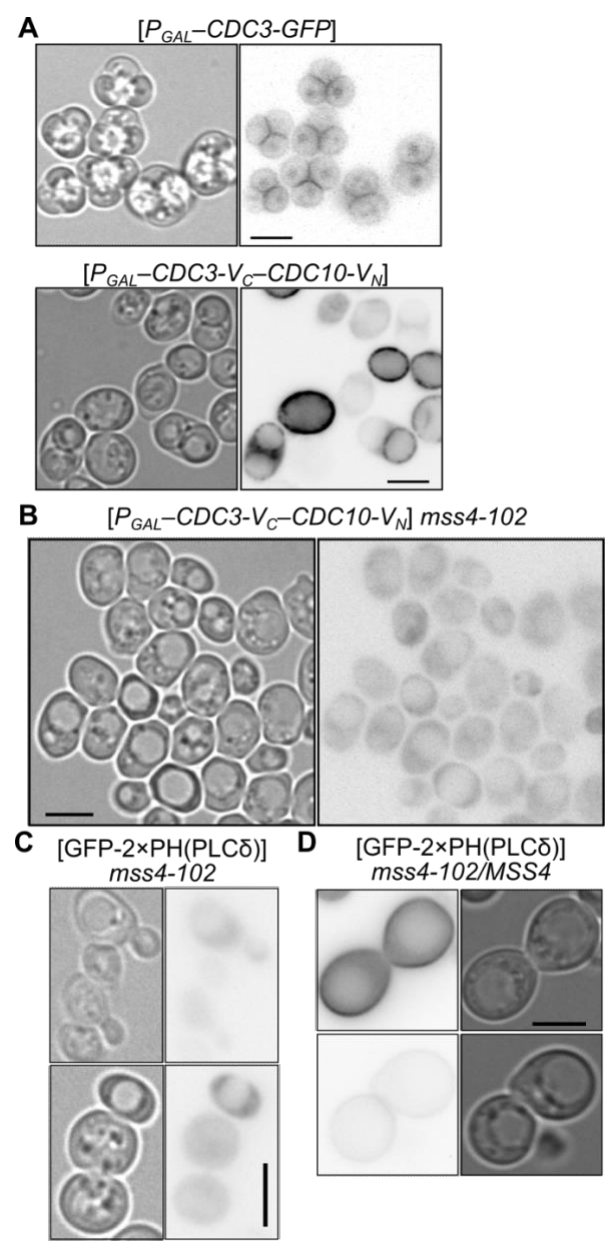


Figure 6. Co-overexpression of Cdc3-V_C and Cdc10 perturbs septin function in sporulation and requires phosphotidylinositol-4,5-bis-phosphate (Pl(4,5)P₂) for plasma membrane mislocalization. (A) Cells of diploid strain H07172 carrying the indicated plasmids ("[P_{GAL} –CDC3-GFP]", pMVB1; "[P_{GAL} –CDC3- V_C –CDC10- V_N ", E00432) were induced to sporulate and transcribe P_{GAL} by culturing in sporulation medium containing 1 uM estradiol for 5 days at 22°C, then imaged for GFP or BiFC signal and transmitted light. GFP LED cube 100% intensity, 250-msec exposure. (B-C) Cells were imaged for GFP fluorescence and transmitted light following overnight culture at 22°C in plasmid-selective liquid medium with 2% galactose. Images were inverted for clarity. (B) mss4-102 strain CBY06598 carrying plasmid E00432. GFP LED cube 100% intensity, 250-msec exposure. (C) mss4-102 strain CBY06598 carrying plasmid pRS426GFP-2×PH(PLCδ). GFP LED cube 90% intensity, 250-msec exposure. (D) Cells from (C) were mated with wild-type haploid strain BY4742 by mixing on the surface of a rich agar plate and then mated cells were used to inoculate plasmid-selective liquid medium with 2% galactose. Cells were imaged after overnight culture at 22°C. GFP LED cube 70% intensity, 250-msec exposure. Scale bars, 5 μm.

Evidence for higher-order polymerization by PM-localized co-overexpressed Cdc3 and Cdc10

The weak $PI(4,5)P_2$ affinity of any individual septin prevents monomers from localizing to the PM, and even septin hetero-octamers dissociate from membranes unless/until they polymerize into filaments with collectively strong PM avidity (Tanaka-Takiguchi et al., 2009; Bridges et al., 2014). Accordingly, whether or not yeast septins at the PM are polymerized into filaments has previously been assessed by fluorescence recovery after photobleaching (FRAP) (Caviston et al., 2003; Dobbelaere et al., 2003). Recovery/exchange is seen when the septin ring is still forming prior to bud emergence but not once the bud has emerged and before the hourglass-shaped septin "collar" splits into two rings. This period coincides with the stage at which arrays of septin filaments are found (Byers and Goetsch, 1976; Ong et al., 2014). Using P_{GAL} -overexpressed Cdc3-GFP, we recapitulated the lack of recovery/exchange in septin collars (Figure 7A), and found a similar lack of recovery/exchange in the PM-localized GFP signal resulting from P_{GAL} co-overexpression of Cdc3-Vc and Cdc10-GFP from the same plasmid (Figure 7B). These data suggest that Cdc3—Cdc10 PM localization involves oligomerization/polymerization into higher-order assemblies.

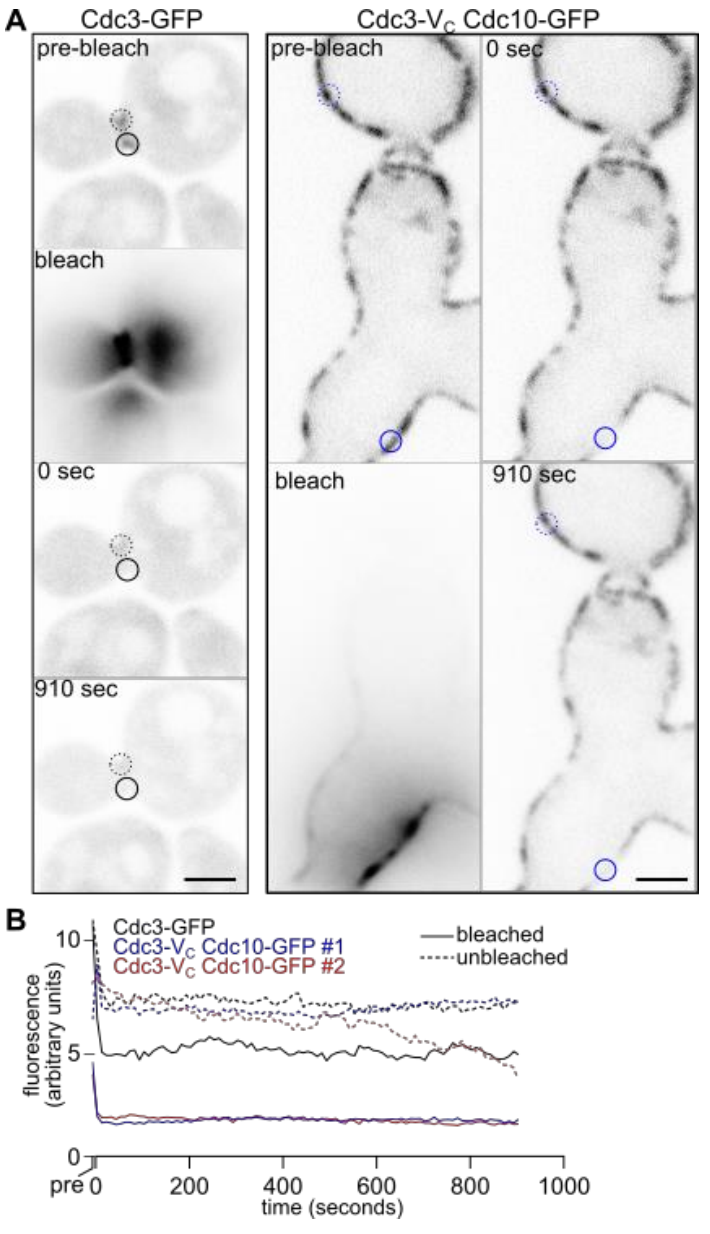


Figure 7. Lack of mobility/cytoplasmic exchange of PM-associated Cdc3-V_C–Cdc10 complexes. (A) Cells of strain BY4741 carrying pMVB1 ("Cdc3-GFP") or G01271 ("Cdc3-V_C Cdc10-GFP") were cultured in plasmid-selective medium containing 2% galactose and then imaged for GFP signal ("pre-bleach"). The areas circled with solid lines were then photobleached. The "bleach" images were captured during the photobleaching. Fluorescence intensity was quantified within those areas (and, as a control, within unbleached areas circled with dashed lines) every 10 seconds for 900 seconds thereafter. Images were inverted for clarity. (B) Fluorescence intensity of the areas in (A), plus areas from another Cdc3-V_C Cdc10-GFP cell (red lines), plotted with time. Scale bars, 2 μm.

DISCUSSION

The original impetus to create a BiFC co-overexpression plasmid was to monitor the kinetics of septin complex assembly in vivo, but our results suggest that septin folding

and assembly are not the rate-limiting steps toward generating fluorescence. For unsplit GFP, we presume that fluorophore maturation is on a similar time scale as septin synthesis/folding/assembly, such that slowing septin folding detectably slows signal accumulation. The added time required to reconstitute the split YFP may decrease the temporal sensitivity of the assay, such that slower septin folding makes an undetectable contribution to signal accumulation kinetics. Thus our single-plasmid BiFC approach may only be useful to detect severe septin folding/assembly defects. Since too severe a defect would slow or stop cell division, this assay may have a narrow range of utility.

The unexpected PM localization and interference with endogenous septin function provided an opportunity for us to learn more about what normally regulates septin complex assembly and membrane association. While we are left with many unanswered questions, we propose the following model (Figure 8). For co-overexpression from a single plasmid, initiation of transcription in both directions from P_{GAL} ensures that for every Cdc3-Vc mRNA, there is one Cdc10 mRNA. In fact, in 2% galactose each burst of P_{GAL} transcription produces >10 nascent mRNAs, with multiple bursts within a 30-minute period (Lenstra et al., 2015). If the mRNAs are translated with similar efficiency, then a given cell could rapidly accumulate enough Cdc3-Vc and Cdc10 to assemble hundreds or thousands of hetero-oligomers. Only Cdc3-Vc—Cdc10 hetero-oligomers, and not homo-oligomers, are competent for PM localization. For P_{GAL} co-overexpression from distinct plasmids, it is less likely that both septins are expressed at similar amounts, Cdc3-Vc—Cdc10 encounters are less common, and PM localization is correspondingly less frequent.

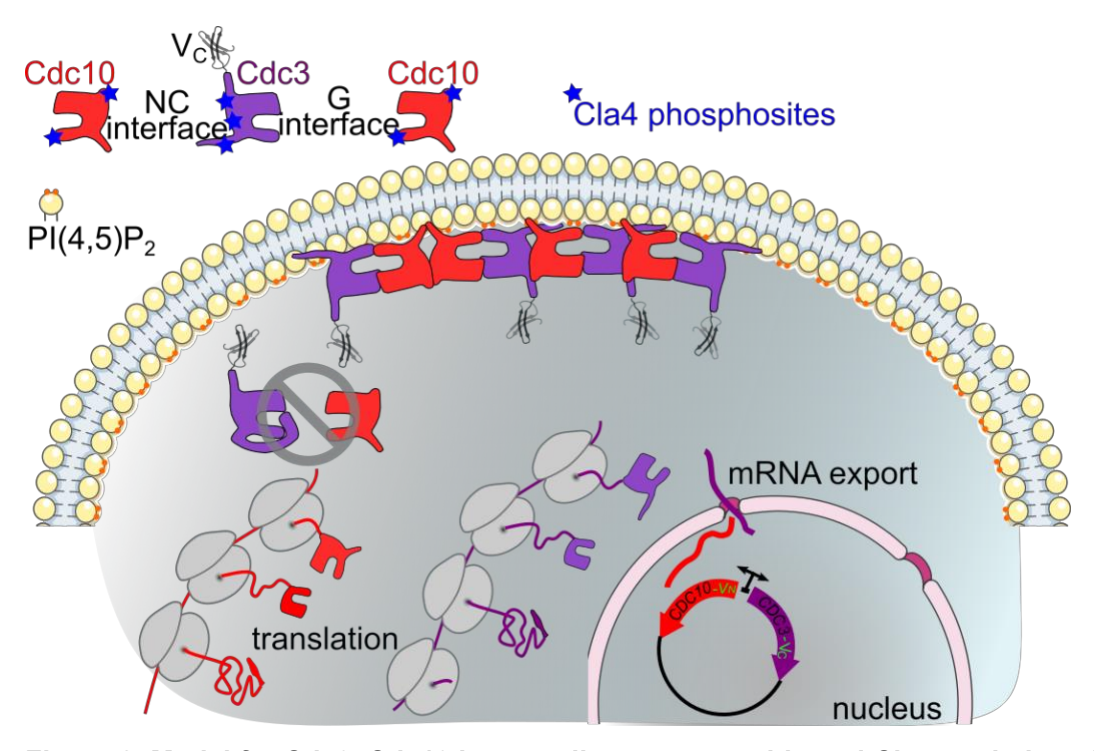


Figure 8. Model for Cdc3–Cdc10 hetero-oligomer assembly and Cla4- and phospholipid-dependent plasma membrane localization. Cartoon illustrations of septins Cdc3 (purple) and Cdc10 (red) are shown with the G interface and Cdc3 NTE diagrammed at top left. Putative and known sites of phosphorylation by Cla4 are illustrated near the interfaces. Cla4 phosphorylation and the $V_{\rm C}$ fusion to the C terminus of Cdc3 favor NC interaction with Cdc10, which repositions the NTE of Cdc3 to allow G-dimerization with other molecules of Cdc10. Cdc10 NC-mediated homodimerization can further contribute to the assembly of long oligomers capable of stable association with PI(4,5)P₂ in the PM via the polybasic region of Cdc10. Coordinated, bidirectional P_{GAL} transcription of BiFC-tagged Cdc3 and Cdc10 promotes the synchrony of mRNA export and subsequent translation, favoring assembly by the tagged septins, though occasional incorporation of endogenous Cdc10 sequesters it away from essential hetero-octameric assemblies containing other septins and capable of forming filaments at the bud neck.

Apart from the stoichiometry $per\ se$, the kinetics/timing of assembly is also likely to be important. We recently developed an assay for post-translational septin assembly in which we transiently overexpressed a single tagged septin from P_{GAL} , then shut off new assembly (Hassell et al., 2022). The excess septin — super-stoichiometric to the endogenous septins — remained diffusely localized in the cytoplasm/nucleus, ostensibly "waiting" until newly-synthesized partner septins were synthesized and, via $de\ novo\$ folding, became available for new complex assembly (Hassell et al., 2022). In the meantime, the excess septins were kept assembly-competent by specific cytosolic chaperones, which we proposed to "protect" the excess septins' dimerization interfaces from inappropriate interactions (Hassell et al., 2022). In particular, our data pointed to

chaperone occupancy of the "G" interface that surrounds and encompasses each septin's guanine nucleotide binding pocket (Sirajuddin et al., 2007; Johnson et al., 2015; Hassell et al., 2022). If, rather than having to wait for them, plenty of molecules of the G-dimer partner are immediately available, then two partner septins simultaneously in excess to the others — and in 1:1 stoichiometry to each other — could rapidly outcompete the chaperones to form a stable dimer. In a native hetero-octamer, Cdc3 and Cdc10 form a G heterodimer and Cdc10 forms a homodimer via the other ("NC") interface (Sirajuddin et al., 2007; Bertin et al., 2008). Thus if many assembly-competent molecules of Cdc3 and Cdc10 became available at the same time, Cdc3—Cdc10—Cdc10—Cdc3 heterotetramers could assemble rather efficiently.

However, our FRAP data do not seem consistent with PM-associated tetramers, and instead point to some kind of higher-order polymer. Furthermore, we previously published evidence that, at endogenous expression levels, the intrinsically disordered NTE of Cdc3 occupies the G interface of newly-synthesized Cdc3 and prevents it from interacting with Cdc10 until Cdc3 has first interacted with Cdc12 via the NC interface, which re-positions the NTE away from the Cdc3–Cdc10 interface (Weems and McMurray, 2017). NTE interference presumably explains why Cdc3 and Cdc10 do not efficiently interact when co-expressed in *E. coli* (Versele et al., 2004). The NTE is adjacent to the α 0 helix (residues 102-116), which undergoes a "domain swap" with the α 0 helix of Cdc12 (Valadares et al., 2017; Cavini et al., 2021) (Figure 8). If Cdc12 is not involved in the excess Cdc3–Cdc10 assembly, then what repositions the Cdc3 NTE?

While using the AlphaFold Multimer tool (Evans et al., 2022) to predict the structures of yeast septin homo- and hetero-dimers, we noticed that the two highest-ranked models for the Cdc3–Cdc10 heterodimer unexpectedly involve the NC interface (Figure S4). In these models, the Cdc3 α 0 helix swaps with that of Cdc10. Cdc3–Cdc10 NC interaction would expose two G interfaces for subsequent oligomerization events, providing a pathway to assembly of long polymers that could stably associate with the PM (Figure 8). We note that, in addition to a Cdc10 residue in a key part of the G interface (Ser256), Cla4 phosphorylates Cdc10 Ser312 (Versele and Thorner, 2004), which is

conspicuously near the predicted NC interface with Cdc3 (Figure S4). Indeed, the side chain of Lys440 in Cdc3 is ~10 Å away, such that phosphorylation at Ser312 could introduce a long-range electrostatic interaction (Figure S4). Cla4 also phosphorylates Cdc3 (Versele and Thorner, 2004), and the four Ser residues in Cdc3 that match the sequence context of known Cla4 substrates (RXS) also cluster near the Cdc3–Cdc10 NC interface (Figure S4). Thus a requirement for Cla4-mediated Cdc3 and/or Cdc10 phosphorylation in NC-interface-mediated Cdc3–Cdc10 oligomerization could explain why Cdc3 and Cdc10 do not appear to oligomerize the same way when co-overexpressed in *E. coli* or *cla4*Δ yeast. Gin4 does not appear to phosphorylate Cdc3 or Cdc10 (Versele and Thorner, 2004), and its only known septin substrate, Shs1, was not found at the PM (Figure 3I). However, by phosphorylating a non-septin protein, Gin4 regulates the function of PM "flippases" that control which lipids are exposed on which PM leaflet (Roelants et al., 2015). The loss of PM localization in *gin4*Δ mutants may reflect changes in PM lipid composition that alter the availability of PI(4,5)P₂ for binding. We propose that the polybasic region of Cdc10 mediates PI(4,5)P₂ binding.

How the 108-residue Vc tag promotes PM localization is mysterious, as we are unaware of any prior evidence that suggests propensity for PM association. One possibility is that, being located near the normal location of direct interaction between the C-terminal extensions of Cdc3 and Cdc12 (Versele et al., 2004), it interferes with NC heterodimerization with Cdc12, and thereby indirectly favors Cdc3–Cdc10 NC interaction. The idea that co-overexpressed Cdc3-Vc and Cdc10 may interact nonnatively via the NC interface provides a plausible explanation for the specificity of endogenous Cdc10 mis-localization. The endogenous Cdc3 we examined was not Vctagged (it was tagged with mCherry), so either it was not competent to co-assemble with the excess Cdc10, or it was able to co-assemble but those assemblies were not competent to localize to the PM. We favor the former explanation, for the following reason: if the presence of a few Cdc3-mCherry (or untagged Cdc3) molecules in an assembly containing mostly Cdc3-Vc and Cdc10-V_N was enough to block PM localization, then we should have seen a loss of PM BiFC signal in the cells expressing endogenous Cdc3-mCherry. The fact that endogenous Cdc3 lacking a Vc tag neither

participated in, nor interfered with, PM mislocalization points to a requirement for the V_{C} tag in a specific kind of interaction with Cdc10 (see above), not in PM mislocalization per se.

In the absence of any Cdc10 overexpression, nearly a third of cells expressing Cdc3-Vc as the sole source of Cdc3 were elongated (Table 1). Moreover, Cdc10 sequestration alone cannot explain the elongated cells we see upon co-overexpression, because at 22°C in the strain background in which we performed most of our experiments (BY4741) viable *cdc10*∆ cells are mostly round (McMurray et al., 2011). Thus a parsimonious explanation for the severe elongation of most wild-type cells co-overexpressing Cdc3-V_C and Cdc10-V_N is that it represents a defect in the assembly of functional septin hetero-octamers due to combination of Cdc10 sequestration and incorporation of V_Ctagged Cdc3. The requirement for Cdc10 in normal septin function can be bypassed by the small molecule guanidine hydrochloride (GdnHCl), which drives an alternative septin complex assembly pathway in which non-native Cdc3 homodimerization allows Cdc10less hexamer assembly by the other septins (McMurray et al., 2011; Johnson et al., 2020). Consistent with septin dysfunction resulting from more than sequestration of endogenous Cdc10, addition of 3 mM GdnHCl to the medium did not block PM localization (Figure S5) and did not ameliorate the elongated morphologies resulting from Cdc3-V_C and Cdc10-V_N co-overexpression (Table 1).

The septin complexes normally made during sporulation contain Cdc3 and Cdc10 but not Cdc12 or Shs1 (McMurray and Thorner, 2008; Garcia et al., 2016), and instead contain Spr28 and Spr3 (Garcia et al., 2016), the sporulation-specific counterpart of Cdc12. Spr3 also has a predicted AH with unknown contributions to curvature preference (McMurray, 2019). Spr3 is required for uniform PM localization by Cdc3 in spores (Pablo-Hernando et al., 2008) but since Spr3 is not expressed in vegetatively dividing cells, it cannot explain the BiFC PM localization we observe upon co-overexpression of Cdc3 and Cdc10 in vegetative cells. Thus while direct evidence for yeast septin AH-mediated PM curvature preference in vivo is lacking, it seems possible that curvature-insensitive PM localization of co-overexpressed Cdc3 and Cdc10 could

represent assembly of a septin complex that lacks the two subunits with AHs known to impart curvature preference in vitro. Like the elongated buds we saw in vegetative cells, the severe sporulation defect we saw upon co-overexpression of Cdc3-Vc and Cdc10-V_N presumably reflects compounding dysfunctions resulting from replacement of untagged Cdc3 in canonical septin hetero-octamers plus sequestration of untagged Cdc10 into non-functional Cdc3–Cdc10 hetero-oligomers.

The large number of human septin genes and splice isoforms thereof provide the potential for a huge variety of septin complexes with distinct properties tailored to the needs of individual human cell types. While the abnormal PM localization that we describe here resulted from genetic engineering in the lab, coordinating the synchrony and extent of septin transcription may be yet another means by which human cells fine-tune septin complex assembly, localization and function. In human cancers, individual septins are often highly overexpressed relative to other septins (Angelis and Spiliotis, 2016). By adding small domains to the N terminus, the inclusion of alternative exons can shift the partner septins with which overexpressed human Septin 9 co-assembles (Devlin et al., 2021). Cancer cells may benefit from the assembly of non-canonical septin complexes driven by septin co-overexpression and "extra" domains added to a flexible septin tail, akin to what we serendipitously found with a synthetic tag.

REFERENCES

- Amberg, D., D. Burke, and J. Strathern. 2005. Methods in Yeast Genetics: A Cold Spring Harbor Laboratory Course Manual, 2005 Edition. Cold Spring Harbor Laboratory Press.
- Angelis, D., and E.T. Spiliotis. 2016. Septin Mutations in Human Cancers. *Front. Cell Dev. Biol.* 4:122. doi:10.3389/fcell.2016.00122.
- Asano, S., J.-E. Park, L.-R. Yu, M. Zhou, K. Sakchaisri, C.J. Park, Y.H. Kang, J. Thorner, T.D. Veenstra, and K.S. Lee. 2006. Direct phosphorylation and activation of a Nim1-related kinase Gin4 by Elm1 in budding yeast. *J. Biol. Chem.* 281:27090–27098. doi:10.1074/jbc.M601483200.
- Barral, Y., V. Mermall, M.S. Mooseker, and M. Snyder. 2000. Compartmentalization of the cell cortex by septins is required for maintenance of cell polarity in yeast. *Mol. Cell*. 5:841–51.

- Barral, Y., M. Parra, S. Bidlingmaier, and M. Snyder. 1999. Nim1-related kinases coordinate cell cycle progression with the organization of the peripheral cytoskeleton in yeast. *Genes Dev.* 13:176–187.
- Barve, G., S. Sridhar, A. Aher, M.H. Sahani, S. Chinchwadkar, S. Singh, L. K N, M.A. McMurray, and R. Manjithaya. 2018. Septins are involved at the early stages of macroautophagy in S. cerevisiae. *J. Cell Sci.* 131:jcs209098. doi:10.1242/jcs.209098.
- Beber, A., C. Taveneau, M. Nania, F.-C. Tsai, A. Di Cicco, P. Bassereau, D. Lévy, J.T. Cabral, H. Isambert, S. Mangenot, and A. Bertin. 2019. Membrane reshaping by micrometric curvature sensitive septin filaments. *Nat. Commun.* 10. doi:10.1038/s41467-019-08344-5.
- Beites, C.L., H. Xie, R. Bowser, and W.S. Trimble. 1999. The septin CDCrel-1 binds syntaxin and inhibits exocytosis. *Nat. Neurosci.* 2:434–439. doi:10.1038/8100.
- Bertin, A., M.A. McMurray, P. Grob, S.-S. Park, G. Garcia, I. Patanwala, H.-L. Ng, T. Alber, J. Thorner, and E. Nogales. 2008. Saccharomyces cerevisiae septins: supramolecular organization of heterooligomers and the mechanism of filament assembly. *Proc. Natl. Acad. Sci. U. S. A.* 105:8274–9. doi:10.1073/pnas.0803330105.
- Bertin, A., M.A. McMurray, L. Thai, G. Garcia, V. Votin, P. Grob, T. Allyn, J. Thorner, and E. Nogales. 2010. Phosphatidylinositol-4,5-bisphosphate promotes budding yeast septin filament assembly and organization. *J. Mol. Biol.* 404:711–731. doi:10.1016/j.jmb.2010.10.002.
- Bouquin, N., Y. Barral, R. Courbeyrette, M. Blondel, M. Snyder, and C. Mann. 2000. Regulation of cytokinesis by the Elm1 protein kinase in Saccharomyces cerevisiae. *J. Cell Sci.* 113 (Pt 8):1435–1445. doi:10.1242/jcs.113.8.1435.
- Bridges, A.A., H. Zhang, S.B. Mehta, P. Occhipinti, T. Tani, and A.S. Gladfelter. 2014. Septin assemblies form by diffusion-driven annealing on membranes. *Proc. Natl. Acad. Sci. U. S. A.* 111:2146–2151. doi:10.1073/pnas.1314138111.
- Byers, B., and L. Goetsch. 1976. A highly ordered ring of membrane-associated filaments in budding yeast. *J. Cell Biol.* 69:717–21.
- Cannon, K.S., B.L. Woods, J.M. Crutchley, and A.S. Gladfelter. 2019. An amphipathic helix enables septins to sense micrometer-scale membrane curvature. *J Cell Biol.* jcb.201807211. doi:10.1083/jcb.201807211.
- Casamayor, A., and M. Snyder. 2003. Molecular Dissection of a Yeast Septin: Distinct Domains Are Required for Septin Interaction, Localization, and Function. *Mol Cell Biol*. 23:2762–2777. doi:10.1128/MCB.23.8.2762-2777.2003.
- Cavini, I.A., D.A. Leonardo, H.V.D. Rosa, D.K.S.V. Castro, H. D'Muniz Pereira, N.F. Valadares, A.P.U. Araujo, and R.C. Garratt. 2021. The Structural Biology of Septins and Their Filaments: An Update. *Front. Cell Dev. Biol.* 9:765085. doi:10.3389/fcell.2021.765085.

- Caviston, J.P., M. Longtine, J.R. Pringle, and E. Bi. 2003. The role of Cdc42p GTPase-activating proteins in assembly of the septin ring in yeast. *Mol. Biol. Cell.* 14:4051–66. doi:10.1091/mbc.E03-04-0247.
- Cvrcková, F., C.D. Virgilio, E. Manser, J.R. Pringle, and K. Nasmyth. 1995. Ste20-like protein kinases are required for normal localization of cell growth and for cytokinesis in budding yeast. *Genes Dev.* 9:1817–1830. doi:10.1101/gad.9.15.1817.
- DeMay, B.S., N. Noda, A.S. Gladfelter, and R. Oldenbourg. 2011. Rapid and quantitative imaging of excitation polarized fluorescence reveals ordered septin dynamics in live yeast. *Biophys. J.* 101:985–994. doi:10.1016/j.bpj.2011.07.008.
- Denney, A.S., A.D. Weems, and M.A. McMurray. 2021. Selective functional inhibition of a tumor-derived p53 mutant by cytosolic chaperones identified using split-YFP in budding yeast. *G3 Bethesda Md*. 11:jkab230. doi:10.1093/g3journal/jkab230.
- Desrivières, S., F.T. Cooke, P.J. Parker, and M.N. Hall. 1998. MSS4, a phosphatidylinositol-4-phosphate 5-kinase required for organization of the actin cytoskeleton in Saccharomyces cerevisiae. *J. Biol. Chem.* 273:15787–15793. doi:10.1074/jbc.273.25.15787.
- Devlin, L., J. Okletey, G. Perkins, J.R. Bowen, K. Nakos, C. Montagna, and E.T. Spiliotis. 2021. Proteomic profiling of the oncogenic septin 9 reveals isoform-specific interactions in breast cancer cells. *Proteomics*. 21:e2100155. doi:10.1002/pmic.202100155.
- Dobbelaere, J., M.S. Gentry, R.L. Hallberg, and Y. Barral. 2003. Phosphorylation-dependent regulation of septin dynamics during the cell cycle. *Dev. Cell.* 4:345–57.
- Dolat, L., and E.T. Spiliotis. 2016. Septins promote macropinosome maturation and traffic to the lysosome by facilitating membrane fusion. *J. Cell Biol.* 214:517–527. doi:10.1083/jcb.201603030.
- Elison, G.L., Y. Xue, R. Song, and M. Acar. 2018. Insights into Bidirectional Gene Expression Control Using the Canonical GAL1/GAL10 Promoter. *Cell Rep.* 25:737-748.e4. doi:10.1016/j.celrep.2018.09.050.
- Evans, R., M. O'Neill, A. Pritzel, N. Antropova, A. Senior, T. Green, A. Žídek, R. Bates, S. Blackwell, J. Yim, O. Ronneberger, S. Bodenstein, M. Zielinski, A. Bridgland, A. Potapenko, A. Cowie, K. Tunyasuvunakool, R. Jain, E. Clancy, P. Kohli, J. Jumper, and D. Hassabis. 2022. Protein complex prediction with AlphaFold-Multimer. 2021.10.04.463034. doi:10.1101/2021.10.04.463034.
- Fares, H., L. Goetsch, and J.R. Pringle. 1996. Identification of a developmentally regulated septin and involvement of the septins in spore formation in Saccharomyces cerevisiae. *J. Cell Biol.* 132:399–411.
- Finnigan, G.C., J. Takagi, C. Cho, and J. Thorner. 2015. Comprehensive Genetic Analysis of Paralogous Terminal Septin Subunits Shs1 and Cdc11 in Saccharomyces cerevisiae. *Genetics*. 200:821–841. doi:10.1534/genetics.115.176495.

- Garcia, G., G.C. Finnigan, L.R. Heasley, S.M. Sterling, A. Aggarwal, C.G. Pearson, E. Nogales, M.A. McMurray, and J. Thorner. 2016. Assembly, molecular organization, and membrane-binding properties of development-specific septins. *J. Cell Biol.* 212:515–529. doi:10.1083/jcb.201511029.
- Garrenton, L.S., C.J. Stefan, M.A. McMurray, S.D. Emr, and J. Thorner. 2010. Pheromone-induced anisotropy in yeast plasma membrane phosphatidylinositol-4,5-bisphosphate distribution is required for MAPK signaling. *Proc. Natl. Acad. Sci. U. S. A.* 107:11805–11810. doi:10.1073/pnas.1005817107.
- Hartwell, L.H. 1971. Genetic control of the cell division cycle in yeast. IV. Genes controlling bud emergence and cytokinesis. *Exp. Cell Res.* 69:265–276.
- Hassell, D., A. Denney, E. Singer, A. Benson, A. Roth, J. Ceglowski, M. Steingesser, and M. McMurray. 2022. Chaperone requirements for de novo folding of Saccharomyces cerevisiae septins. *Mol. Biol. Cell.* 33:ar111. doi:10.1091/mbc.E22-07-0262.
- Heasley, L.R., and M.A. McMurray. 2016. Roles of septins in prospore membrane morphogenesis and spore wall assembly in Saccharomyces cerevisiae. *Mol. Biol. Cell*. 27:442–450. doi:10.1091/mbc.E15-10-0721.
- Homma, K., S. Terui, M. Minemura, H. Qadota, Y. Anraku, Y. Kanaho, and Y. Ohya. 1998. Phosphatidylinositol-4-phosphate 5-kinase localized on the plasma membrane is essential for yeast cell morphogenesis. *J. Biol. Chem.* 273:15779–15786. doi:10.1074/jbc.273.25.15779.
- Huh, W.-K., J.V. Falvo, L.C. Gerke, A.S. Carroll, R.W. Howson, J.S. Weissman, and E.K. O'Shea. 2003. Global analysis of protein localization in budding yeast. *Nature*. 425:686–691. doi:10.1038/nature02026.
- Ibanes, S., F. El-Alaoui, J. Lai-Kee-Him, C. Cazevieille, F. Hoh, S. Lyonnais, P. Bron, L. Cipelletti, L. Picas, and S. Piatti. 2022. The Syp1/FCHo2 protein induces septin filament bundling through its intrinsically disordered domain. *Cell Rep.* 41:111765. doi:10.1016/j.celrep.2022.111765.
- Iwase, M., J. Luo, S. Nagaraj, M. Longtine, H.B. Kim, B.K. Haarer, C. Caruso, Z. Tong, J.R. Pringle, and E. Bi. 2006. Role of a Cdc42p effector pathway in recruitment of the yeast septins to the presumptive bud site. *Mol. Biol. Cell.* 17:1110–1125. doi:10.1091/mbc.E05-08-0793.
- Iwase, M., S. Okada, T. Oguchi, and A. Toh-e. 2004. Forchlorfenuron, a phenylurea cytokinin, disturbs septin organization in Saccharomyces cerevisiae. *Genes Genet. Syst.* 79:199–206.
- Jiao, F., K.S. Cannon, Y.-C. Lin, A.S. Gladfelter, and S. Scheuring. 2020. The hierarchical assembly of septins revealed by high-speed AFM. *Nat. Commun.* 11:5062. doi:10.1038/s41467-020-18778-x.
- Johnson, C.R., M.G. Steingesser, A.D. Weems, A. Khan, A. Gladfelter, A. Bertin, and M.A. McMurray. 2020. Guanidine hydrochloride reactivates an ancient septin hetero-oligomer assembly pathway in budding yeast. *eLife*. 9:e54355. doi:10.7554/eLife.54355.

- Johnson, C.R., A.D. Weems, J.M. Brewer, J. Thorner, and M.A. McMurray. 2015. Cytosolic chaperones mediate quality control of higher-order septin assembly in budding yeast. *Mol. Biol. Cell.* doi:10.1091/mbc.E14-11-1531.
- Kim, H., B. Haarer, and J. Pringle. 1991. Cellular morphogenesis in the Saccharomyces cerevisiae cell cycle: localization of the CDC3 gene product and the timing of events at the budding site. *J Cell Biol*. 112:535–544. doi:10.1083/jcb.112.4.535.
- Kloimwieder, A., and F. Winston. 2011. A Screen for Germination Mutants in Saccharomyces cerevisiae. *G3 Genes Genomes Genet.* 1:143–149. doi:10.1534/g3.111.000323.
- Lenstra, T.L., A. Coulon, C.C. Chow, and D.R. Larson. 2015. Single-Molecule Imaging Reveals a Switch between Spurious and Functional ncRNA Transcription. *Mol. Cell*. 60:597–610. doi:10.1016/j.molcel.2015.09.028.
- Lew, D.J. 2003. The morphogenesis checkpoint: how yeast cells watch their figures. *Curr. Opin. Cell Biol.* 15:648–653.
- Li, Z., F.J. Vizeacoumar, S. Bahr, J. Li, J. Warringer, F.S. Vizeacoumar, R. Min, B. Vandersluis, J. Bellay, M. Devit, J.A. Fleming, A. Stephens, J. Haase, Z.-Y. Lin, A. Baryshnikova, H. Lu, Z. Yan, K. Jin, S. Barker, A. Datti, G. Giaever, C. Nislow, C. Bulawa, C.L. Myers, M. Costanzo, A.-C. Gingras, Z. Zhang, A. Blomberg, K. Bloom, B. Andrews, and C. Boone. 2011. Systematic exploration of essential yeast gene function with temperature-sensitive mutants. *Nat. Biotechnol.* 29:361–367. doi:10.1038/nbt.1832.
- Longtine, M.S., H. Fares, and J.R. Pringle. 1998. Role of the yeast Gin4p protein kinase in septin assembly and the relationship between septin assembly and septin function. *J. Cell Biol.* 143:719–36.
- Longtine, M.S., C.L. Theesfeld, J.N. McMillan, E. Weaver, J.R. Pringle, and D.J. Lew. 2000. Septin-Dependent Assembly of a Cell Cycle-Regulatory Module in Saccharomyces cerevisiae. *Mol. Cell. Biol.* 20:4049–4061. doi:10.1128/MCB.20.11.4049-4061.2000.
- Marquardt, J., L.-L. Yao, H. Okada, T. Svitkina, and E. Bi. 2020. The LKB1-like Kinase Elm1 Controls Septin Hourglass Assembly and Stability by Regulating Filament Pairing. *Curr. Biol. CB*. 30:2386-2394.e4. doi:10.1016/j.cub.2020.04.035.
- McMurray, M.A. 2016. Assays for genetic dissection of septin filament assembly in yeast, from de novo folding through polymerization. *Methods Cell Biol.* 136:99–116. doi:10.1016/bs.mcb.2016.03.012.
- McMurray, M.A. 2019. The long and short of membrane curvature sensing by septins. *J. Cell Biol.* 218:1083–1085. doi:10.1083/jcb.201903045.
- McMurray, M.A., A. Bertin, G. Garcia 3rd, L. Lam, E. Nogales, and J. Thorner. 2011. Septin filament formation is essential in budding yeast. *Dev. Cell*. 20:540–549. doi:10.1016/j.devcel.2011.02.004.
- McMurray, M.A., and J. Thorner. 2008. Septin stability and recycling during dynamic structural transitions in cell division and development. *Curr. Biol. CB*. 18:1203–1208. doi:10.1016/j.cub.2008.07.020.

- McQuilken, M., M.S. Jentzsch, A. Verma, S.B. Mehta, R. Oldenbourg, and A.S. Gladfelter. 2017. Analysis of Septin Reorganization at Cytokinesis Using Polarized Fluorescence Microscopy. *Front. Cell Dev. Biol.* 5:42. doi:10.3389/fcell.2017.00042.
- Mendonça, D.C., S.L. Guimarães, H.D. Pereira, A.A. Pinto, M.A. de Farias, A.S. de Godoy, A.P.U. Araujo, M. van Heel, R.V. Portugal, and R.C. Garratt. 2021. An atomic model for the human septin hexamer by cryo-EM. *J. Mol. Biol.* 433:167096. doi:10.1016/j.jmb.2021.167096.
- Mirdita, M., K. Schütze, Y. Moriwaki, L. Heo, S. Ovchinnikov, and M. Steinegger. 2022. ColabFold: making protein folding accessible to all. *Nat. Methods*. 19:679–682. doi:10.1038/s41592-022-01488-1.
- Nagaraj, S., A. Rajendran, C.E. Jackson, and M.S. Longtine. 2008. Role of nucleotide binding in septin-septin interactions and septin localization in Saccharomyces cerevisiae. *Mol. Cell. Biol.* 28:5120–5137. doi:10.1128/MCB.00786-08.
- Ni, L., and M. Snyder. 2001. A genomic study of the bipolar bud site selection pattern in Saccharomyces cerevisiae. *Mol. Biol. Cell.* 12:2147–2170. doi:10.1091/mbc.12.7.2147.
- Oh, Y., J. Schreiter, R. Nishihama, C. Wloka, and E. Bi. 2013. Targeting and functional mechanisms of the cytokinesis-related F-BAR protein Hof1 during the cell cycle. *Mol. Biol. Cell*. 24:1305–1320. doi:10.1091/mbc.E12-11-0804.
- Ong, K., C. Wloka, S. Okada, T. Svitkina, and E. Bi. 2014. Architecture and dynamic remodelling of the septin cytoskeleton during the cell cycle. *Nat. Commun.* 5:5698. doi:10.1038/ncomms6698.
- Pablo-Hernando, M.E., Y. Arnaiz-Pita, H. Tachikawa, F. del Rey, A.M. Neiman, and C.R. Vázquez de Aldana. 2008. Septins localize to microtubules during nutritional limitation in Saccharomyces cerevisiae. *BMC Cell Biol.* 9:55. doi:10.1186/1471-2121-9-55.
- Pagliuso, A., T.N. Tham, J.K. Stevens, T. Lagache, R. Persson, A. Salles, J.-C. Olivo-Marin, S. Oddos, A. Spang, P. Cossart, and F. Stavru. 2016. A role for septin 2 in Drp1-mediated mitochondrial fission. *EMBO Rep.* 17:858–873. doi:10.15252/embr.201541612.
- Patasi, C., J. Godočíková, S. Michlíková, Y. Nie, R. Káčeriková, K. Kválová, S. Raunser, and M. Farkašovský. 2015. The role of Bni5 in the regulation of septin higher-order structure formation. *Biol. Chem.* 396:1325–1337. doi:10.1515/hsz-2015-0165.
- Rodríguez-Escudero, I., F.M. Roelants, J. Thorner, C. Nombela, M. Molina, and V.J. Cid. 2005. Reconstitution of the mammalian PI3K/PTEN/Akt pathway in yeast. *Biochem. J.* 390:613–23. doi:10.1042/BJ20050574.
- Roelants, F.M., B.M. Su, J. von Wulffen, S. Ramachandran, E. Sartorel, A.E. Trott, and J. Thorner. 2015. Protein kinase Gin4 negatively regulates flippase function and controls plasma membrane asymmetry. *J. Cell Biol.* 208:299–311. doi:10.1083/jcb.201410076.
- Sadian, Y., C. Gatsogiannis, C. Patasi, O. Hofnagel, R.S. Goody, M. Farkasovsky, and S. Raunser. 2013. The role of Cdc42 and Gic1 in the regulation of septin filament formation and dissociation. *eLife*. 2. doi:10.7554/eLife.01085.

- Schaefer, R.M., L.R. Heasley, D.J. Odde, and M.A. McMurray. 2016. Kinetic partitioning during de novo septin filament assembly creates a critical G1 "window of opportunity" for mutant septin function. *Cell Cycle Georget. Tex.* 0. doi:10.1080/15384101.2016.1196304.
- Schindelin, J., I. Arganda-Carreras, E. Frise, V. Kaynig, M. Longair, T. Pietzsch, S. Preibisch, C. Rueden, S. Saalfeld, B. Schmid, J.-Y. Tinevez, D.J. White, V. Hartenstein, K. Eliceiri, P. Tomancak, and A. Cardona. 2012. Fiji: an open-source platform for biological-image analysis. *Nat. Methods*. 9:676–682. doi:10.1038/nmeth.2019.
- Schmidt, M., A. Varma, T. Drgon, B. Bowers, and E. Cabib. 2003. Septins, under Cla4p regulation, and the chitin ring are required for neck integrity in budding yeast. *Mol. Biol. Cell.* 14:2128–2141. doi:10.1091/mbc.e02-08-0547.
- Sharma, S., A. Quintana, G.M. Findlay, M. Mettlen, B. Baust, M. Jain, R. Nilsson, A. Rao, and P.G. Hogan. 2013. An siRNA screen for NFAT activation identifies septins as coordinators of store-operated Ca2+ entry. *Nature*. 499:238–242. doi:10.1038/nature12229.
- Shi, W., K.S. Cannon, B.N. Curtis, C. Edelmaier, A.S. Gladfelter, and E. Nazockdast. 2023. Curvature sensing as an emergent property of multiscale assembly of septins. *Proc. Natl. Acad. Sci. U. S. A.* 120:e2208253120. doi:10.1073/pnas.2208253120.
- Shulewitz, M.J., C.J. Inouye, and J. Thorner. 1999. HsI7 localizes to a septin ring and serves as an adapter in a regulatory pathway that relieves tyrosine phosphorylation of Cdc28 protein kinase in Saccharomyces cerevisiae. *Mol. Cell. Biol.* 19:7123–7137. doi:10.1128/MCB.19.10.7123.
- Sirajuddin, M., M. Farkasovsky, F. Hauer, D. Kühlmann, I.G. Macara, M. Weyand, H. Stark, and A. Wittinghofer. 2007. Structural insight into filament formation by mammalian septins. *Nature*. 449:311–5. doi:10.1038/nature06052.
- Sopko, R., D. Huang, N. Preston, G. Chua, B. Papp, K. Kafadar, M. Snyder, S.G. Oliver, M. Cyert, T.R. Hughes, C. Boone, and B. Andrews. 2006. Mapping pathways and phenotypes by systematic gene overexpression. *Mol. Cell.* 21:319–330. doi:10.1016/j.molcel.2005.12.011.
- Stefan, C.J., A. Audhya, and S.D. Emr. 2002. The yeast synaptojanin-like proteins control the cellular distribution of phosphatidylinositol (4,5)-bisphosphate. *Mol. Biol. Cell.* 13:542–557. doi:10.1091/mbc.01-10-0476.
- Tanaka-Takiguchi, Y., M. Kinoshita, and K. Takiguchi. 2009. Septin-mediated uniform bracing of phospholipid membranes. *Curr. Biol. CB*. 19:140–5. doi:10.1016/j.cub.2008.12.030.
- Tóth, V., H. Vadászi, L. Ravasz, D. Mittli, D. Mátyás, T. Molnár, A. Micsonai, T. Szaniszló, P. Lőrincz, R.Á. Kovács, T. Juhász, T. Beke-Somfai, G. Juhász, B.A. Györffy, K.A. Kékesi, and J. Kardos. 2022. Neuronal-specific septin-3 binds Atg8/LC3B, accumulates and localizes to autophagosomes during induced autophagy. *Cell. Mol. Life Sci. CMLS*. 79:471. doi:10.1007/s00018-022-04488-8.

- Valadares, N.F., H. d' Muniz Pereira, A.P. Ulian Araujo, and R.C. Garratt. 2017. Septin structure and filament assembly. *Biophys. Rev.* 9:481–500. doi:10.1007/s12551-017-0320-4.
- Veatch, J.R., M.A. McMurray, Z.W. Nelson, and D.E. Gottschling. 2009. Mitochondrial dysfunction leads to nuclear genome instability via an iron-sulfur cluster defect. *Cell*. 137:1247–1258. doi:10.1016/j.cell.2009.04.014.
- Versele, M., B. Gullbrand, M.J. Shulewitz, V.J. Cid, S. Bahmanyar, R.E. Chen, P. Barth, T. Alber, and J. Thorner. 2004. Protein-protein interactions governing septin heteropentamer assembly and septin filament organization in Saccharomyces cerevisiae. *Mol. Biol. Cell.* 15:4568–83. doi:10.1091/mbc.E04-04-0330.
- Versele, M., and J. Thorner. 2004. Septin collar formation in budding yeast requires GTP binding and direct phosphorylation by the PAK, Cla4. *J. Cell Biol.* 164:701–15. doi:10.1083/jcb.200312070.
- Vrabioiu, A.M., and T.J. Mitchison. 2006. Structural insights into yeast septin organization from polarized fluorescence microscopy. *Nature*. 443:466–9. doi:10.1038/nature05109.
- Weems, A.D., C.R. Johnson, J.L. Argueso, and M.A. McMurray. 2014. Higher-Order Septin Assembly Is Driven by GTP-Promoted Conformational Changes: Evidence From Unbiased Mutational Analysis in Saccharomyces cerevisiae. *Genetics*. 196:711–727. doi:10.1534/genetics.114.161182.
- Weems, A.D., and M.A. McMurray. 2017. The step-wise pathway of septin hetero-octamer assembly in budding yeast. *eLife*. 6. doi:10.7554/eLife.23689.
- Winzeler, E.A., D.D. Shoemaker, A. Astromoff, H. Liang, K. Anderson, B. Andre, R. Bangham, R. Benito, J.D. Boeke, H. Bussey, A.M. Chu, C. Connelly, K. Davis, F. Dietrich, S.W. Dow, M.E. Bakkoury, F. Foury, S.H. Friend, E. Gentalen, G. Giaever, J.H. Hegemann, T. Jones, M. Laub, H. Liao, N. Liebundguth, D.J. Lockhart, A. Lucau-Danila, M. Lussier, N. M'Rabet, P. Menard, M. Mittmann, C. Pai, C. Rebischung, J.L. Revuelta, L. Riles, C.J. Roberts, P. Ross-MacDonald, B. Scherens, M. Snyder, S. Sookhai-Mahadeo, R.K. Storms, S. Véronneau, M. Voet, G. Volckaert, T.R. Ward, R. Wysocki, G.S. Yen, K. Yu, K. Zimmermann, P. Philippsen, M. Johnston, and R.W. Davis. 1999. Functional Characterization of the S. cerevisiae Genome by Gene Deletion and Parallel Analysis. *Science*. 285:901–906. doi:10.1126/science.285.5429.901.
- Wloka, C., R. Nishihama, M. Onishi, Y. Oh, J. Hanna, J.R. Pringle, M. Krauss, and E. Bi. 2011. Evidence that a septin diffusion barrier is dispensable for cytokinesis in budding yeast. *Biol. Chem.* 392:813–829. doi:10.1515/BC.2011.083.
- Woods, B.L., K.S. Cannon, E.J.D. Vogt, J.M. Crutchley, and A.S. Gladfelter. 2021. Interplay of septin amphipathic helices in sensing membrane-curvature and filament bundling. *Mol. Biol. Cell.* 32:br5. doi:10.1091/mbc.E20-05-0303.
- Zhang, J., C. Kong, H. Xie, P.S. McPherson, S. Grinstein, and W.S. Trimble. 1999.

 Phosphatidylinositol polyphosphate binding to the mammalian septin H5 is modulated by GTP. *Curr. Biol. CB*. 9:1458–1467.